

Optimal configurations of the Deep Underground Neutrino Experiment

Vernon Barger*

Department of Physics, University of Wisconsin, Madison, WI 53706, USA

Atri Bhattacharya†

Department of Physics, University of Arizona, Tucson, AZ 85721, USA

Animesh Chatterjee‡

University of Texas at Arlington, Arlington, TX 76019, USA

Raj Gandhi§

Harish-Chandra Research Institute, Chhatnag Road, Jhansi, Allahabad 211 019, India

Danny Marfatia¶

Department of Physics and Astronomy, University of Hawaii at Manoa, Honolulu, HI 96822, USA

Mehedi Masud||

Harish-Chandra Research Institute, Chhatnag Road, Jhansi, Allahabad 211 019, India

We perform a comprehensive study of the ability of the Deep Underground Neutrino Experiment (DUNE) to answer outstanding questions in the neutrino sector. We consider the sensitivities to the mass hierarchy, the octant of θ_{23} and to CP violation using data from beam and atmospheric neutrinos. We evaluate the dependencies on the precision with which θ_{13} will be measured by reactor experiments, on the detector size, beam power and exposure time, on detector magnetization, and on the systematic uncertainties achievable with and without a near detector. We find that a 35 kt far detector in DUNE with a near detector will resolve the eight-fold degeneracy that is intrinsic to long baseline experiments and will meet the primary goals of oscillation physics that it is designed for.

*barger@pheno.wisc.edu

†atrib@email.arizona.edu

‡animesh.chatterjee@uta.edu

§nubarnu@gmail.com

¶dmarf8@hawaii.edu

||masud@hri.res.in

Table 1. Best fit values of the oscillation parameters.²

Parameter	Best fit value
$\sin^2 \theta_{12}$	0.307
$\sin^2 \theta_{13}$	0.0241
$\sin^2 \theta_{23}$ (lower octant)	0.427
$\sin^2 \theta_{23}$ (higher octant)	0.613
Δm_{21}^2	$7.54 \times 10^{-5} \text{ eV}^2$
$ \Delta m_{31}^2 $	$2.43 \times 10^{-3} \text{ eV}^2$
δ_{CP}	0

1. Introduction

Neutrino oscillations have by now been conclusively established by several pioneering experiments. It is now understood that the mixing between the three neutrino flavors is governed by the so-called PMNS mixing matrix,

$$U_{\text{PMNS}} = \begin{pmatrix} c_{12}c_{13} & s_{12}c_{13} & s_{13}e^{-i\delta_{CP}} \\ -s_{12}c_{23} - c_{12}s_{13}s_{23}e^{i\delta_{CP}} & c_{12}c_{23} - s_{12}s_{13}s_{23}e^{i\delta_{CP}} & c_{13}s_{23} \\ s_{12}s_{23} - c_{12}s_{13}c_{23}e^{i\delta_{CP}} & -c_{12}s_{23} - s_{12}s_{13}c_{23}e^{i\delta_{CP}} & c_{13}c_{23} \end{pmatrix}, \quad (1)$$

and the mass-squared differences: $\Delta m_{31}^2 = m_3^2 - m_1^2$ and Δm_{21}^2 . Here, c_{ij} and s_{ij} are $\cos \theta_{ij}$ and $\sin \theta_{ij}$ respectively, for the three mixing angles θ_{12} , θ_{23} and θ_{13} , and δ_{CP} is a (Dirac) CP phase. While solar and atmospheric neutrino experiments have determined the first two mixing angles quite precisely, reactor experiments have made remarkable progress in determining θ_{13} .¹ (See Table 1 for the values of the oscillation parameters used in our work.)

Now that θ_{13} has been conclusively shown to be non-zero and not too small,^{1,3} the focus of neutrino oscillation experiments has shifted to the measurement of δ_{CP} that determines whether or not oscillating neutrinos violate CP. A second important unanswered question for model building is whether the mass hierarchy is *normal* with $\Delta m_{31}^2 > 0$, or *inverted* with $\Delta m_{31}^2 < 0$. Finally, the question of whether θ_{23} is larger or smaller than $\pi/4$ bears on models based on lepton symmetries.

An effort towards resolving the above issues and thereby taking us a step closer to completing our knowledge of the neutrino mass matrix, is the Deep Underground Neutrino Experiment (DUNE).^a DUNE will employ a large liquid argon far detector (FD). It is expected to be placed underground in the Homestake mine at a distance of 1300 km from Fermilab, from which a neutrino beam will be directed towards the detector. Large-mass Liquid Argon Time Projection Chambers (LAr-TPCs) have unprecedented capabilities for the detection of neutrino interactions due to precise and sensitive spatial and calorimetric resolution. However, the final configuration

^aThe inputs we use, and the corresponding references, pertain to the erstwhile Long Baseline Neutrino Experiment (LBNE),^{4,5} which has undergone a new phase of internationalisation and expansion. This has led to a change in the name of the experiment, to DUNE. Nonetheless, it is expected that the configuration we assume here vis a vis fluxes, baseline and energies will remain largely intact.

of the experiment is still under discussion.^{6,7} The sensitivity of DUNE to the mass hierarchy, to CP violation and to the octant of θ_{23} depends on, among other things, how well other oscillation parameters are known, on the amount of data that can be taken in a reasonable time frame, on the systematic uncertainties that compromise the data, and on the charge discrimination capability of the detector. Our goal (in this extension of our previous work⁷) is to study how these factors affect DUNE in various experimental configurations. Other recent studies of some of the physics capabilities of DUNE can be found in Ref.⁸.

1.1. Objectives

The various considerations of our work are motivated by possible configurations for DUNE in the initial phase of its program. The initial stage of DUNE will, at the very least, permit the construction of an unmagnetized 10 kt FD underground. Several improvements upon this basic configuration are under consideration. These might include

- upgrading the FD to 35 kt for improved statistics,
- having a precision near detector (ND) for better calibration of the initial flux and reducing the involved systematic uncertainties,
- magnetizing the FD to make it possible to distinguish between particles and antiparticles in the atmospheric neutrino flux.^b

It must be noted that some of the above upgrades would also have supplementary benefits — an ND, for example, will also allow precision studies of the involved neutrino nucleon cross sections, thereby reducing present uncertainties.

Since it might not be feasible to combine all of the above upgrades into an initial DUNE configuration, we evaluate which combination would be most beneficial as far as the physics of neutrino oscillations is concerned. Specifically, we study the following experimental configurations:

- (1) A beam experiment with and without an ND.
- (2) An atmospheric neutrino experiment.
- (3) An experiment with and without an ND that combines beam and atmospheric neutrino data collected at the FD.
- (4) A global configuration that combines DUNE data (with and without ND) with NO ν A⁹ and T2K¹⁰ data.

Our study will highlight the benefits of

- (1) building a larger 35 kt FD as opposed to a 10 kt detector,
- (2) higher exposure (kt-MW-yr),¹¹

^bThe beam experiment would have the neutrino and antineutrino runs happen asynchronously. Thus, the events from the two would be naturally distinguished and magnetization of the FD would not affect its results.

Table 2. Systematic uncertainties for signal and background channels in DUNE.^{5,15}

Detector configuration	Systematics	
	Signal	Background
With ND	ν_e : 1% ν_μ : 1%	ν_e : 1% ν_μ : 5%
Without ND	ν_e : 5% ν_μ : 5%	ν_e : 10% ν_μ : 45%

- (3) magnetizing the FD versus having an unmagnetized detector volume,
- (4) utilizing atmospheric neutrinos,
- (5) precision θ_{13} measurements,

Throughout, we estimate how data from NO ν A and T2K improve DUNE sensitivities; for previous discussions see Refs.^{4,12}. All simulations for the beam experiments have been done numerically with the GLOBES software.¹³

2. Experimental specifications and analysis methodology

We consider neutrinos resulting from a 120 GeV proton beam from Fermilab with a beam power of 700 kW and an uptime of 1.65×10^7 seconds per year (or equivalently 6×10^{20} protons on target (POT) per year) incident at a LAr FD at a baseline of 1300 km; an upgrade to a 2.3 MW beam is a possibility. As noted in Ref.¹⁴, the physics performance is roughly equivalent for proton beam energies that exceed 60 GeV. We simulate events at the FD using the GLOBES software¹³ and the fluxes used by the DUNE collaboration.

If the FD is placed underground, it is also sensitive to atmospheric neutrinos. We simulate atmospheric neutrino events (as described in Appendix 7) and both ν_e appearance and ν_μ disappearance channel events from the beam in the neutrino and antineutrino modes with an event reconstruction efficiency of 85%. In our simulation of the DUNE beam experiment we employ the signal and background systematics for ν_e appearance and ν_μ disappearance channels from Refs.^{5,15}; see Table 2.^c For the energy resolutions, we have used the method of bin-based automatic energy smearing with $\frac{\sigma}{E} = \frac{0.20}{\sqrt{E}}$ for ν_μ events and $\frac{\sigma}{E} = \frac{0.15}{E}$ for ν_e events; see the appendix of Ref.⁵ An alternative is to use migration matrices.^{5,12} For NO ν A⁹ and T2K,¹⁰ the relevant parameters are given in Tables 3 and 4, respectively. An up-to-date description of the NO ν A and T2K experiments can be found in Ref.¹².

^cOur ND analysis represents the most obvious benefit that the beam experiment will reap with an ND, *viz.*, improvement in systematics for the signal and background events. In addition, an ND will also improve our understanding of the fluxes and cross sections, thereby reducing shape-related uncertainties in the analysis. We do not attempt an exploration of this facet of the ND because the exact nature of the improvement would depend to a large extent on the specifics of the ND, which for the DUNE is yet in the planning stage. Our ND analysis represents a worst-case scenario for improvement in the systematics.

Table 3. Systematic uncertainties for NO ν A.⁹

Detector configuration	Systematics	
	Signal	Background
15 kt TASD 3 yrs. ν + 3 yrs. $\bar{\nu}$ 6×10^{20} POT/yr with a 700 kW beam	ν_e : 5%	ν_e : 10%
	ν_μ : 2%	ν_μ : 10%

Table 4. Systematic uncertainties for T2K.¹⁰

Detector configuration	Systematics	
	Signal	Background
22.5 kt water Cherenkov 5 yrs. ν 8.3×10^{20} POT/yr with a 770 kW beam	ν_e : 5%	ν_e : 5%
	ν_μ : 5%	ν_μ : 5%

Throughout, we assume that placing the detector underground does not result in a significant change of the signal and background analysis, apart from making the detector also sensitive to the atmospheric neutrino events, and thus allowing a combined analysis of the beam and atmospheric data over the duration of the experiment.

We assume that the beam is run in the neutrino mode for a period of five years, and thereafter in the antineutrino mode for five more years.

For the atmospheric neutrino analysis, and consequently the combined beam and atmospheric analysis, it becomes important to consider both a magnetized and an unmagnetized LAr detector. In the former case, the detector sensitivity, especially for the resolution of the mass hierarchy, is significantly improved over the latter, due to its ability to distinguish between particles and antiparticles. This, however, is only partly applicable to the ν_e events, because for a 10 kt volume detector, it is difficult to distinguish between the tracks arising from of ν_e and $\bar{\nu}_e$ interactions. This difficulty arises because pair-production and bremsstrahlung sets in with increasing energies, and above ≈ 5 GeV, the detector completely loses its ability to distinguish between these CP conjugate pairs. On the other hand, due to their tracks being significantly longer, ν_μ and $\bar{\nu}_\mu$ events are clearly distinguishable at all accessible energies. We implement this in our detector simulation for the atmospheric neutrino and combined analysis.

For our simulation of atmospheric neutrino data, the energy and angular resolutions of the detector are as in Table 5.¹⁶ The atmospheric fluxes are taken from Ref.¹⁷, the flux and systematic uncertainties from Ref.¹⁸, and the density profile of the earth from Ref.¹⁹.

The charge identification capability of the detector is incorporated as discussed in Ref.¹⁶. For electron events, we conservatively assume a 20% probability of charge identification in the energy range 1 – 5 GeV, and no capability for events with energies above 5 GeV. Since the muon charge identification capability of a LAr-

Table 5. Detector parameters used for the analysis of atmospheric neutrinos.¹⁶

Rapidity (y)	0.45 for ν 0.30 for $\bar{\nu}$
Energy Resolution (ΔE)	$\sqrt{(0.01)^2 + (0.15)^2/(yE_\nu) + (0.03)^2}$
Angular Resolution ($\Delta\theta$)	3.2° for ν_μ 2.8° for ν_e
Detector efficiency (\mathcal{E})	85%

TPC is excellent for energies between 1 and 10 GeV, we have assumed it to be 100%.

For the combined analysis of beam and atmospheric events, we first calculate the χ^2 separately from the atmospheric analysis (using our code) and the DUNE beam analysis (using GLoBES) for a set of fixed oscillation parameters. After adding these two fixed parameter χ^2 values, we marginalize over θ_{13} , θ_{23} , $|\Delta m_{31}^2|$ and δ_{CP} to get the minimized χ^2 ; see Appendix 7. The procedure is similar for our combined analysis of DUNE, T2K and NO ν A data.

3. Mass hierarchy

Since δ_{CP} will likely remain undetermined by experiments preceeding DUNE, we analyze the sensitivity to the mass hierarchy as a function of this parameter. The analysis is carried out by assuming one of the hierarchies to be true and then determining by means of a χ^2 test, how well the other hierarchy can be excluded. We marginalize over the present day uncertainties of each of the prior determined parameters.

The δ_{CP} dependence of the sensitivity to the mass hierarchy arises through the oscillation probability,²⁰

$$P_{\mu e} = T_1^2 + T_2^2 + 2T_1T_2 \cos(\delta_{\text{CP}} + \Delta), \quad (2)$$

where,

$$T_1 = \alpha \sin 2\theta_{12} \cos \theta_{23} \frac{\sin(x\Delta)}{x} \quad (3)$$

$$T_2 = \sin 2\theta_{13} \sin \theta_{23} \frac{\sin[(1-x)\Delta]}{(1-x)}, \quad (4)$$

and $\alpha = \frac{\Delta m_{21}^2}{\Delta m_{31}^2}$, $x = \frac{2EV}{\Delta m_{31}^2}$, $\Delta = \frac{\Delta m_{31}^2 L}{4E}$, and $V = \pm 2\sqrt{2}G_F N_e$ is the matter potential (positive for neutrinos and negative for antineutrinos). The only other relevant probability, $P_{\mu\mu}$, is mildly dependent on δ_{CP} .

3.1. Analysis with a 35 kt unmagnetized LAr FD

As is evident from Fig. 1, mass hierarchy resolution benefits significantly from having an ND. But, note that the results with or without an ND are similar for regions of

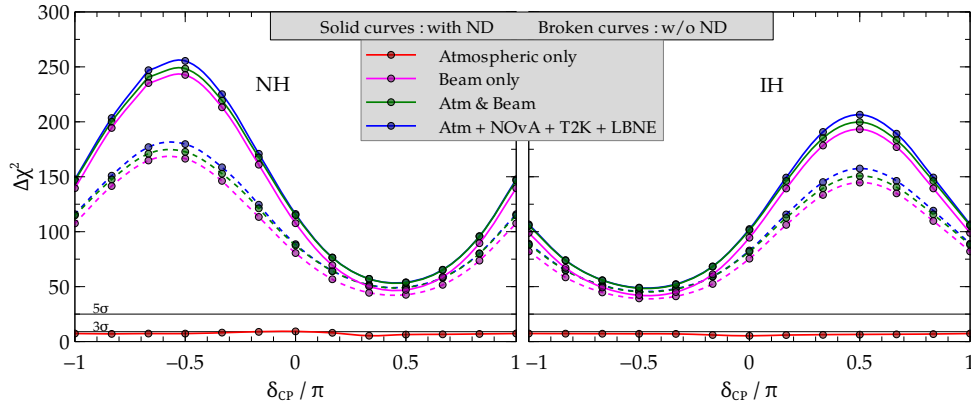


Fig. 1. Sensitivity to the mass hierarchy as a function of true δ_{CP} for a true normal hierarchy (NH) and a true inverted hierarchy (IH) with an 350 kt-yr exposure at the unmagnetized far detector configured with and without a near detector (ND). A run-time of 5 years each (3×10^{21} protons on target) with a ν and $\bar{\nu}$ beam is assumed. The combined sensitivity with NOvA (15 kt T ASD, 3 yrs. ν + 3 yrs. $\bar{\nu}$) and T2K (22.5 kt water cerenkov, 5 yrs. ν) data is also shown.

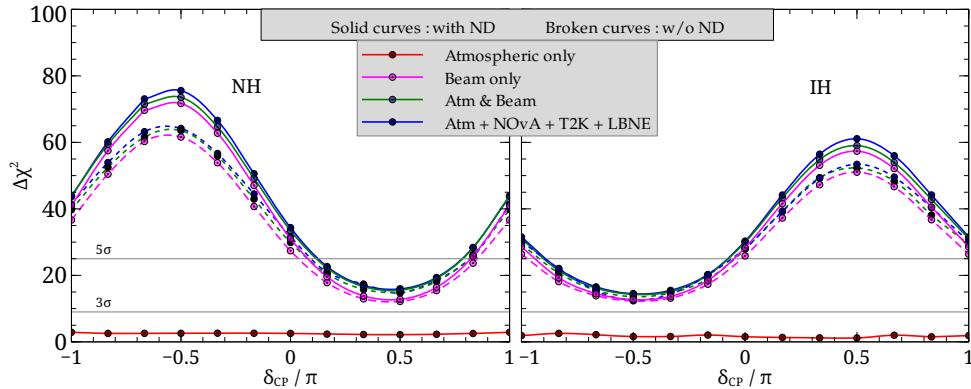


Fig. 2. Similar to Fig. 1 but for a 100 kt-yr unmagnetized LAr FD.

δ_{CP} where the sensitivity is worse ($\delta_{CP} \in [45^\circ, 135^\circ]$ for the normal hierarchy and $\delta_{CP} \in [-135^\circ, -45^\circ]$ for the inverted hierarchy).

Since the wrong hierarchy can be excluded by the DUNE beam-only experiment to significantly more than 5σ with an unmagnetized LAr FD and an exposure of 350 kt-yrs. without the help of ND, the added contributions of both the atmospheric neutrinos, and the better signal and background systematics provided by an ND, are not essential for this measurement.

Similar conclusions vis-a-vis the near detector can be drawn for a 10 kt FD from

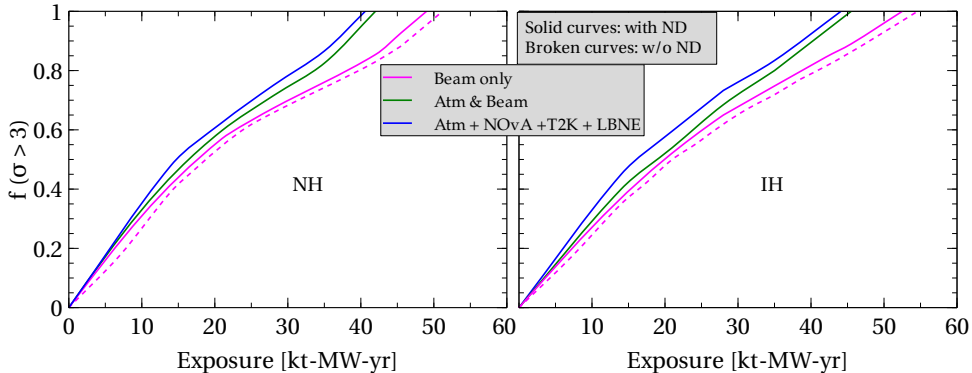


Fig. 3. The fraction of CP phases for which the sensitivity to the mass hierarchy exceeds 3σ as a function of DUNE exposure, for different unmagnetized detector configurations. The time exposure refers to calendar years for DUNE with 1.65×10^7 seconds of uptime per year. The entire $\text{NO}\nu\text{A}$ and T2K datasets are assumed to be available when DUNE starts taking data (and do not contribute to the exposure shown).

Fig. 2. For a 100 kt-yr exposure, the combined analysis resolves the hierarchy to more than 5σ for a large δ_{CP} fraction, and to more than 3σ for all values of δ_{CP} .

3.2. Exposure analysis

We now evaluate the exposure needed to resolve the mass hierarchy for the entire range of δ_{CP} . In Fig. 3, we show the CP fraction ($f(\sigma > 3)$) for which the sensitivity to mass hierarchy is greater than 3σ , as a function of exposure. Salient points evident from Fig. 3 are:

- For a beam only analysis, we see that a 3σ determination of the hierarchy for any δ_{CP} value is possible with a roughly 50 kt-MW-yr exposure. This means the hierarchy can be resolved by a 35 kt FD and a 700 kW beam in two years.
- A near detector does not reduce the exposure needed for a 3σ measurement.
- Information from atmospheric neutrinos reduces the exposure required to about 45 kt-MW-yr.
- A further combination with $\text{NO}\nu\text{A}$ and T2K data provides minor improvement.

3.3. Variation of systematics

In Fig. 4, we show the maximum sensitivity to the mass hierarchy for the entire δ_{CP} (true) space as a function of the exposure. We have allowed for variations in systematics for DUNE with an ND that are 3 times as large or small as those in Table 2). The width of the band produced by this procedure may be considered

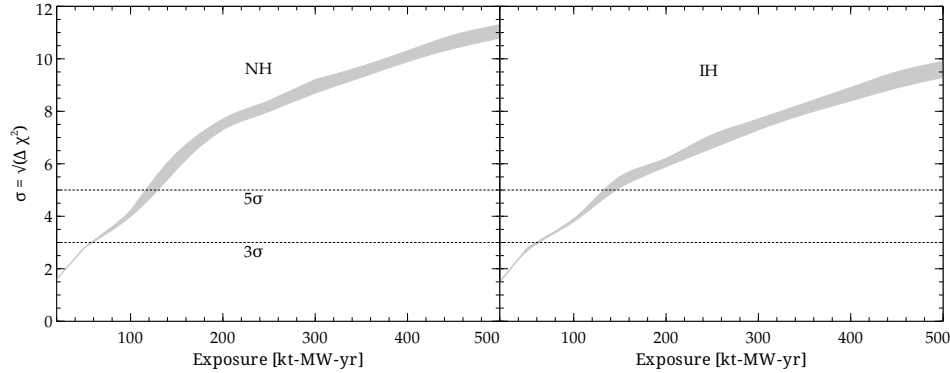


Fig. 4. Maximum sensitivity to the mass hierarchy for all values of δ_{CP} allowing for different systematics (see Sec. 3.3), as a function of exposure. Only beam data (with both an FD and ND) have been considered.

as a measure of the effect of systematics on the hierarchy sensitivity when an ND is used (which seems to be the likely scenario in practice) along with an FD. We observe the following features from Fig. 4:

- For the NH (left panel), both 3σ and 5σ levels of sensitivity can be reached with an exposure of about 50 and 120 kt-MW-yr, respectively. This is consistent with Fig. 3 wherein the solid magenta curve in the left panel reaches unity at roughly 50 kt-MW-yr.
- For exposures below ~ 20 kt-MW-yr, the sensitivity is not statistically significant ($\lesssim 1.5\sigma$).
- The variation of systematics has a small effect on the sensitivities for lower exposures ($\lesssim 100$ kt-MW-yr) and the effect gets slightly magnified for larger exposures, as evident from the widening of the bands.
- The hierarchy sensitivity for a true IH scenario (right panel of Fig. 4) shows qualitatively similar behaviour as that for NH.

3.4. Effect of magnetization

In Fig. 5, we compare the sensitivity to the mass hierarchy of an unmagnetized and magnetized 100 kt-yr LAr FD for a true NH. As discussed earlier, magnetizing the detector volume holds significance for the atmospheric neutrino analysis, since it allows the discrimination of neutrinos and antineutrinos in the flux. Consequently, for the magnetized detector the atmospheric neutrinos alone contribute an almost 3σ sensitivity, thus also enhancing the combined sensitivity; the beam-only results remain unaffected by magnetization.

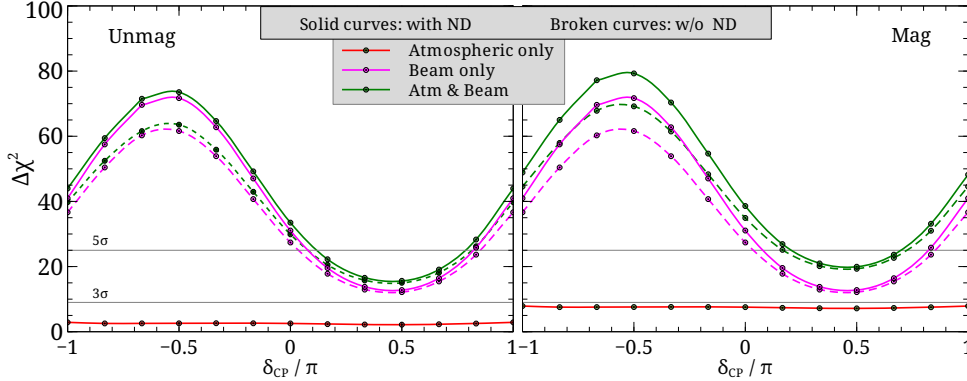


Fig. 5. Sensitivity to the mass hierarchy with a 100 kt-yr exposure with a magnetized (mag) and unmagnetized (unmag) FD. The true hierarchy is normal.

3.5. Some remarks on the results

Some understanding of the qualitative nature of the results may be gleaned from considering the relevant expressions at the level of oscillation probabilities.

Ignoring systematic uncertainties, a *theoretical* event-rate dataset (N^{th}) and an *experimental* one (N^{exp}) can be used to define

$$\chi^2 \sim \sum_i \frac{(N^{\text{th}}(i) - N^{\text{exp}}(i))^2}{N^{\text{exp}}(i)}. \quad (5)$$

Since the event rate at energy E in the e^- appearance channel is given by $P_{\mu e}(E) \times \Phi(E) \times \sigma_{\text{CC}}(E)$, the sensitivity to the mass hierarchy follows the behavior of

$$\Pi^{\text{MH}}(\text{A}, \text{B}) = (P_{\mu e}^{\text{A}} - P_{\mu e}^{\text{B}})^2, \quad (6)$$

where A represents the assumed true hierarchy and B represents the test hierarchy. The opposing natures of the sensitivities seen for the NH as true and IH as true scenarios respectively can be related to the δ_{CP} -dependent phase difference between $\Pi^{\text{MH}}(\text{NH}, \text{IH})$ and $\Pi^{\text{MH}}(\text{IH}, \text{NH})$ at energies where the flux is high, *i.e.*, 1.5–3.5 GeV; see Fig. 16 in Appendix B. The *oscillatory* nature of $\Delta\chi^2$ with respect to δ_{CP} in each case can be traced back to Eq. (6) too.

Because of the strong parameter space degeneracies involved in the appearance channel probability [Eq. (2)], neither the T2K nor the NO ν A experiments are capable of significantly improving the mass hierarchy sensitivities in their respective configurations. It is apparent that the mass hierarchy study benefits immensely from the longer baseline as well as improved systematics of the DUNE set-up as compared to T2K and NO ν A.

Since the mass hierarchy will be determined at 3σ with relatively little exposure (see Fig. 3), henceforth, we assume the mass hierarchy to be known. It is well known

that studies of the octant degeneracy and CP violation benefit significantly from knowledge of the mass hierarchy.

4. Octant degeneracy

We test the sensitivity to the θ_{23} octant by using the true value to be equivalent to the present best-fits $\sin^2(\theta_{23}^{\text{true}}) = 0.427$ (0.613) for the lower (higher) octants (LO/HO), except for Fig. 7, where we show the sensitivities for a range of θ_{23} values in both octants. The $\Delta\chi^2$ in each case represents the sensitivity to disfavoring the opposite octant when a particular choice of $\theta_{23}^{\text{true}}$ is made.

The results for the octant analysis have one important feature — the inverted hierarchy scenario shows almost no variation in sensitivity with δ_{CP} . This follows from the well-known result that when neutrino masses are arranged in an inverted hierarchy, the contribution to the $\Delta\chi^2$ comes almost equally from antineutrinos and neutrinos, but with nearly opposite values of δ_{CP} , while if they conform to the normal hierarchy, the neutrinos dominate over the antineutrinos and the overall result largely traces the features of the neutrino-only $\Delta\chi^2$.

4.1. Analysis with a 35 kt unmagnetized LAr FD

Figure 6 shows the sensitivity to the octant of θ_{23} for a given mass hierarchy.^d By and large, a beam only analysis with an ND provides better sensitivity than the combined analysis with atmospheric data without an ND. Only for the lower octant and normal hierarchy (LO-NH), do the sensitivities almost coincide.

Figure 7 shows the octant sensitivity as a function of true θ_{23} . No sensitivity is expected for $\theta_{23} = 45^\circ$. The sensitivity with an ND is slightly greater than the combined analysis with atmospheric data without an ND if the true hierarchy is inverted, and the converse is true for a normal hierarchy.

4.2. Effect of θ_{13} precision

Resolving the octant degeneracy depends greatly on the precision with which θ_{13} is known. As Fig. 8 shows, a 2% uncertainty on $\sin^2 2\theta_{13}$ significantly improves the octant sensitivity compared to a 5% uncertainty on $\sin^2 2\theta_{13}$.

4.3. Exposure analysis

Results of our exposure analysis are shown separately for the two octants in Figs. 9 and 10. We note the following:

- In the case of LO-NH, for exposures below 50 kt-MW-yr, $f(\sigma > 3)$ rises slowly with exposure for a beam-only experiment with or without a near

^dThe χ^2 analysis converges to the minimum extremely slowly in the HO case of the combined setup. Hence, for results in this section, we only show representative plots for the combined setup for the LO case. We expect qualitatively similar results for the HO case.

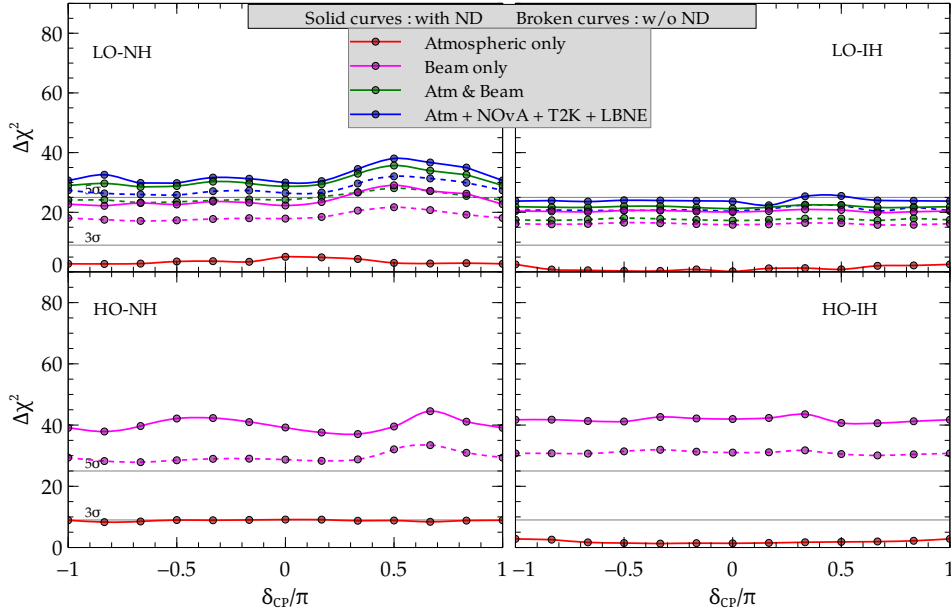


Fig. 6. Sensitivity to the octant of θ_{23} with $\sigma(\sin^2 2\theta_{13}) = 0.05 \times \sin^2 2\theta_{13}$ and $\sin^2 \theta_{23} = 0.427$ in the lower octant (LO) and $\sin^2 \theta_{23} = 0.613$ in the higher octant (HO), for both hierarchies and a 350 kt-yr unmagnetized FD exposure configured with and without an ND. Representative results of the combined sensitivity with atmospheric data, and with $\text{NO}\nu\text{A}$ and T2K are shown for the lower octant.

detector; see Fig. 9. Above this exposure, the curves steepen and eventually the degeneracy is broken for all δ_{CP} values for a 75 kt-MW-yr exposure. Thus, the octant will be known at 3σ in one year after the mass hierarchy is determined with a 35 kt detector and 700 kW beam.

- The right panels of Figs. 9 and 10 show the IH case. The steepness of the curves can be understood from Fig. 6 which shows that $\Delta\chi^2$ is almost independent of δ_{CP} for the IH. As the exposure is increased, $\Delta\chi^2$ increases, and above a critical exposure, the octant degeneracy is broken at 3σ for almost all values of δ_{CP} with a small increment in exposure.
- From Fig. 10, we observe that the lower octant can be ruled out at 3σ for the entire δ_{CP} parameter space with less than a 40 kt-MW-yr exposure, with or without a near detector.

4.4. Variation of systematics

In Fig. 11, we plot the maximum sensitivity to the octant that can be achieved for all values of δ_{CP} . We express the sensitivity as a band, obtained by varying the

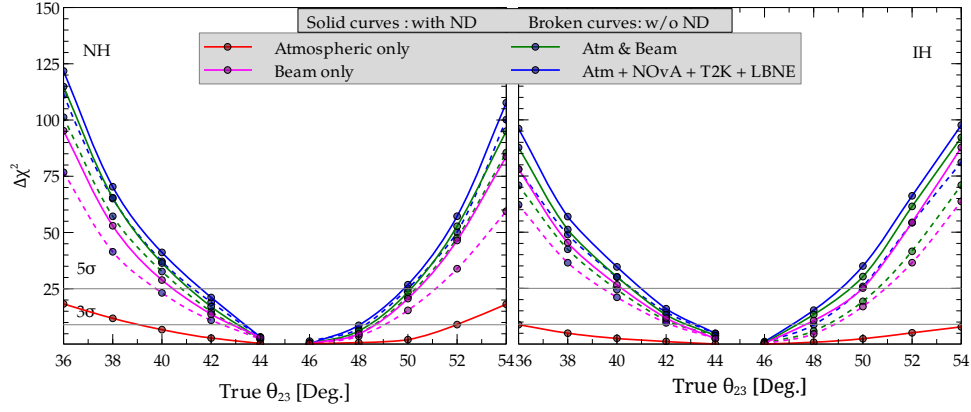


Fig. 7. Sensitivity to the octant for a 350 kt-yr unmagnetized FD exposure as a function of θ_{23} and with $\sigma(\sin^2 2\theta_{13}) = 0.05 \times \sin^2 2\theta_{13}$.

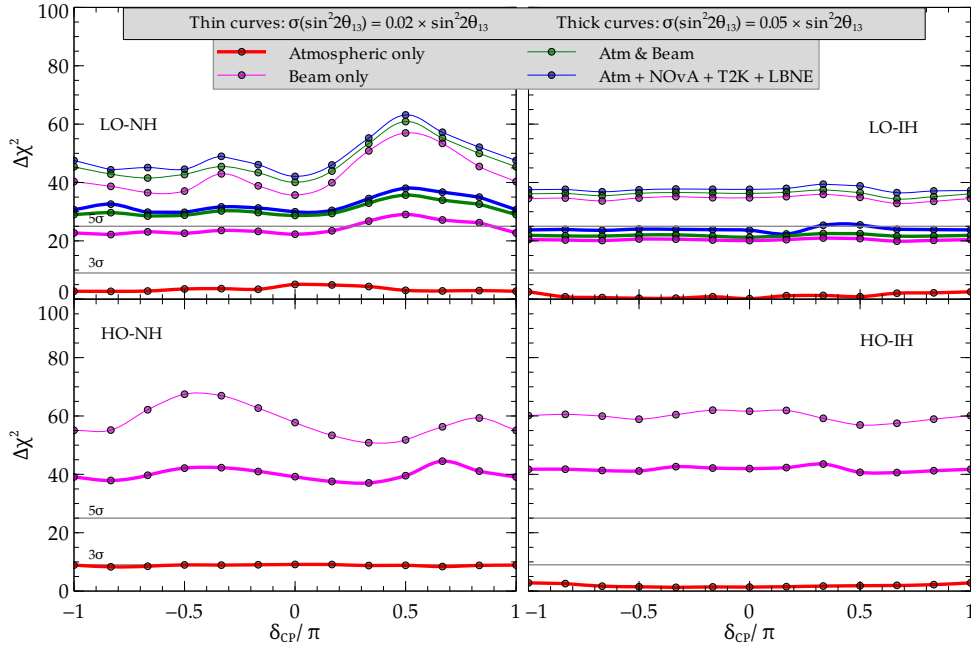


Fig. 8. Octant sensitivity for $\sigma(\sin^2 2\theta_{13}) = 0.02 \times \sin^2 2\theta_{13}$ and $\sigma(\sin^2 2\theta_{13}) = 0.05 \times \sin^2 2\theta_{13}$ for a 350 kt-yr unmagnetized FD and an ND. Representative results of the combined sensitivity with atmospheric data, and with NO ν A and T2K are shown for the lower octant.^a

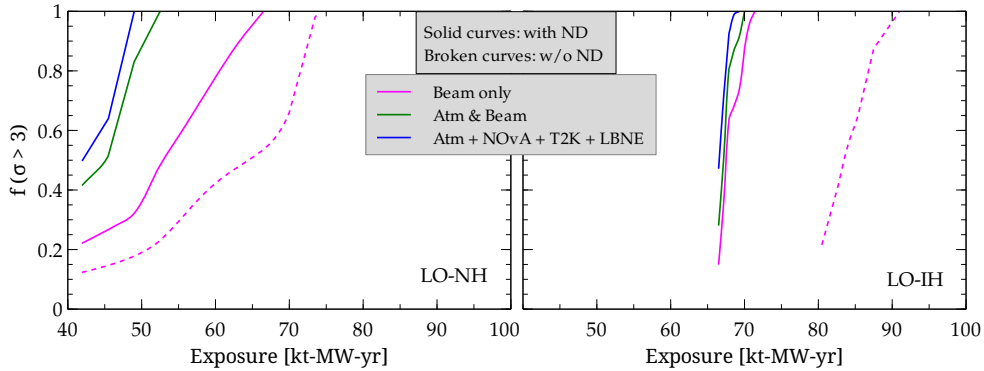


Fig. 9. The fraction of CP phases for which the sensitivity to the octant exceeds 3σ as a function of exposure, for θ_{23} in the lower octant (LO) and $\sigma(\sin^2 2\theta_{13}) = 0.05 \times \sin^2 2\theta_{13}$.

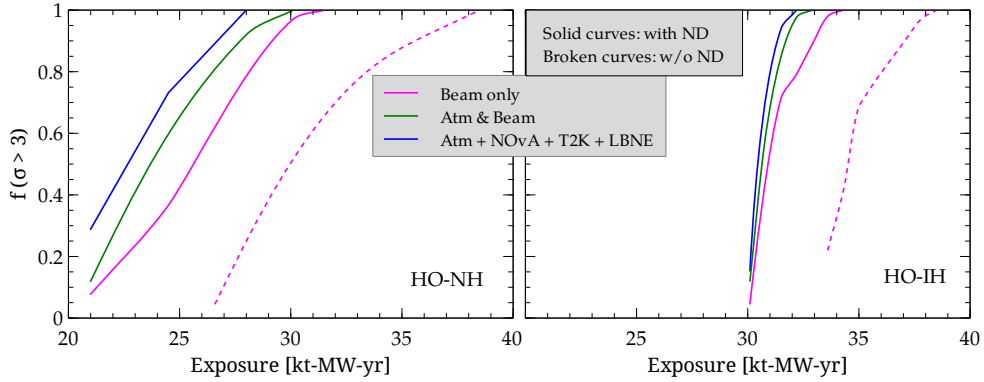


Fig. 10. The fraction of CP phases for which the sensitivity to the octant exceeds 3σ as a function of exposure, for θ_{23} in the higher octant (HO) and $\sigma(\sin^2 2\theta_{13}) = 0.05 \times \sin^2 2\theta_{13}$.

systematics as described in Sec. 3.3). We note from Fig. 11 that,

- The 3σ sensitivity level can be achieved with ~ 70 kt-MW-yr for both hierarchies. This is consistent with Fig. 9.
- For the NH, it takes less (~ 400 kt-MW-yr) exposure to obtain 5σ sensitivity compared to the true IH scenario (~ 500 kt-MW-yr).
- The variation of systematics has a negligible effect on the sensitivity for exposures $\lesssim 70$ kt-MW-yr until 3σ sensitivity is reached. Thereafter, to achieve the 5σ level, the sensitivities get slightly more affected by systematics.

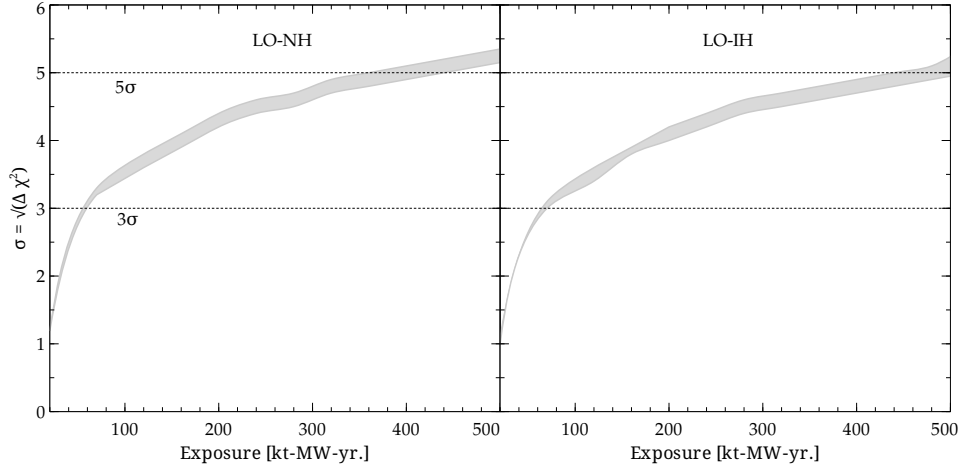


Fig. 11. Similar to Fig. 4, but for the maximum sensitivity to a true lower octant (LO).

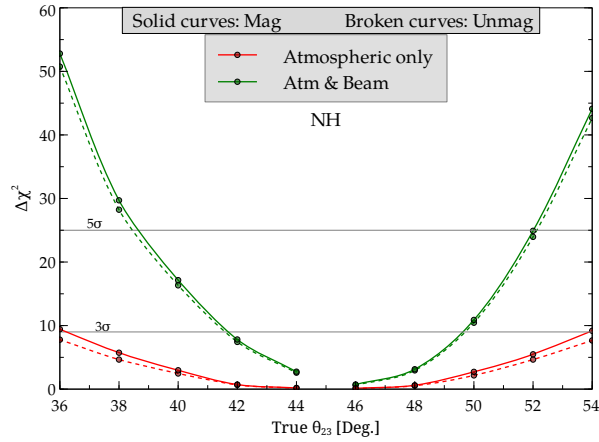


Fig. 12. Octant sensitivity of a magnetized and an unmagnetized detector with a 100 kt-yr exposure. The true hierarchy is assumed to be normal.

4.5. Effect of magnetization

We see from Fig. 12, that magnetizing the detector has almost no effect on the sensitivity to the octant. From a practical standpoint, it is unlikely that a 35 kt FD would be magnetized, with no consequence for octant sensitivity.

It is apparent that the octant resolution benefits significantly from the presence of a calibrating ND. As Figs. 9 and 10 show, the consequent improvement in statistics reduces the runtime required for the achievement of a 3σ significant resolution by

at least 8 yrs (for NH, both octants) and as much as 20 yrs for the LO-IH scenario.

In contrast, the benefit of adding the atmospheric flux is modest, except in the case of LO-NH where a combination of the atmospheric and beam sensitivities can drive the resolution to almost 5σ significance despite the absence of the ND. While the atmospheric contribution is also large in the case of HO-NH, in this case the beam-only experiment is already capable of resolving the degeneracy to more than a 3σ level by itself even without the ND. In the latter case, therefore, the additional expenditure that would be inevitably involved in building the FD underground, would not be justifiable.

The octant degeneracy resolution also greatly benefit from investment in increasing the FD volume to 35 kt from 10 kt, as is evident from the Figs. 9 and 10.

5. CP violation

Of the six oscillation parameters, δ_{CP} is the least well known. Part of the reason for this was the difficulty in experimentally determining the value of θ_{13} . With reactor experiments over the last three years having made significant progress toward the precision determination of the latter, and it being established by now that the value of θ_{13} is non-zero by a fair amount, the precision determination of δ_{CP} in a future experiment should be possible.

In the following we study the sensitivity of the DUNE to CP-violation in the neutrino sector brought about by a non-zero δ_{CP} phase. To determine the $\Delta\chi^2$ that represents the experiment's sensitivity to CP-violation, we assume a test δ_{CP} value of 0 (or π) and compute the $\Delta\chi^2$ for any non-zero (or $\neq \pi$) true δ_{CP} . Since the disappearance channel probability $P_{\mu\mu}$ is only mildly sensitive to the δ_{CP} , CP-violation in the neutrino sector can only be studied by experiments sensitive to the appearance channel $\nu_\mu \rightarrow \nu_e$. It is obvious, given the nature of the latter channel's probability $P_{\mu e}$, that the maximum sensitivity will be due to values of true δ_{CP} close to odd multiples of $\pi/2$.

Due to the non-zero value of θ_{13} being now established, other experiments sensitive to the $\nu_\mu \rightarrow \nu_e$ appearance channel, including the T2K and NO ν A, are also strongly poised to look for CP-violation. Consequently, this is one study where combining data from DUNE, T2K and NO ν A proves to be significantly beneficial.

5.1. Analysis with a 35 kt unmagnetized LAr FD

To study CP violation, reduced systematics courtesy the placement of an ND proves to be beneficial (Fig. 13). Maximal CP violation can be ruled out at more than 5σ by a beam only analysis with a 350 kt-yr exposure in conjunction with the ND. However, 5σ resolution toward ruling out maximal CP-violation can even be achieved despite the absence of an ND by combining results from the T2K, NO ν A and the DUNE.

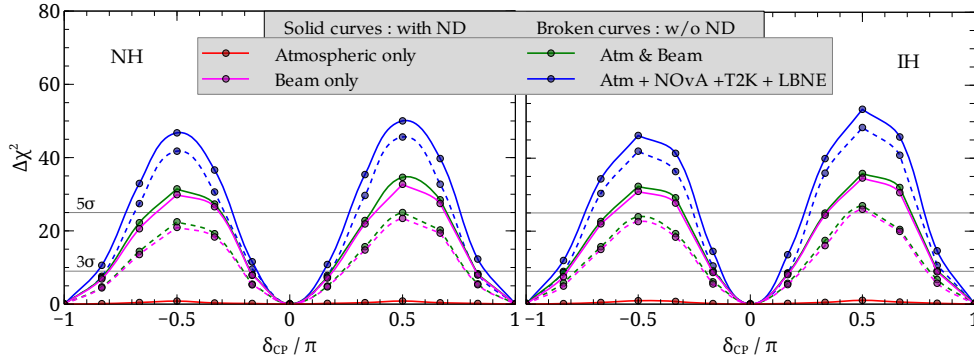


Fig. 13. Sensitivity to CP violation for a 350 kt-yr unmagnetized FD exposure assuming $\sigma(\sin^2 2\theta_{13}) = 0.05 \times \sin^2 2\theta_{13}$.

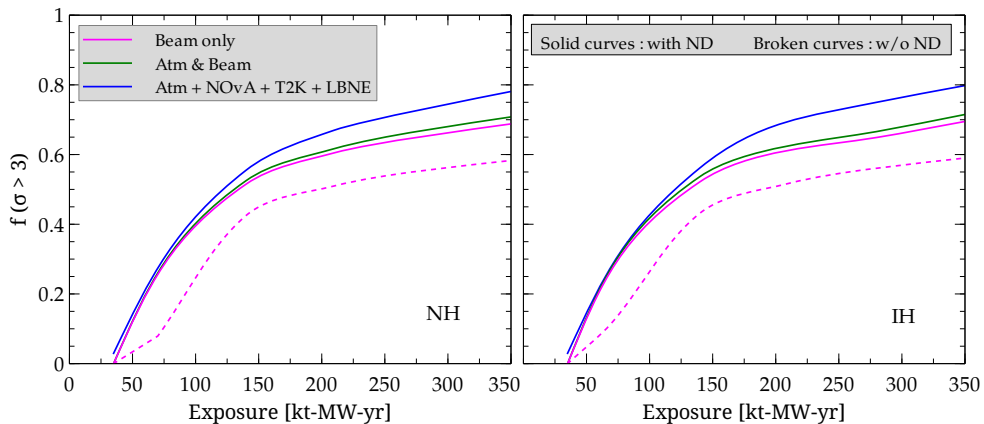


Fig. 14. The fraction of CP phases for which the sensitivity to CPV exceeds 3σ as a function of exposure.

5.2. Exposure analysis

In Fig. 14, we show the CP fraction for which CP violation can be established at 3σ . Needless to say, the CP fraction has to be less than unity since even an almost ideal experiment cannot exclude CP violating values of the phase that are close to the CP conserving values, 0 and π . In the context of CP violation, the CP fraction is a measure of how well an experiment can probe small CP violating effects. From Fig. 14, we find:

- There is no sensitivity to CP violation at the 3σ level for exposures smaller

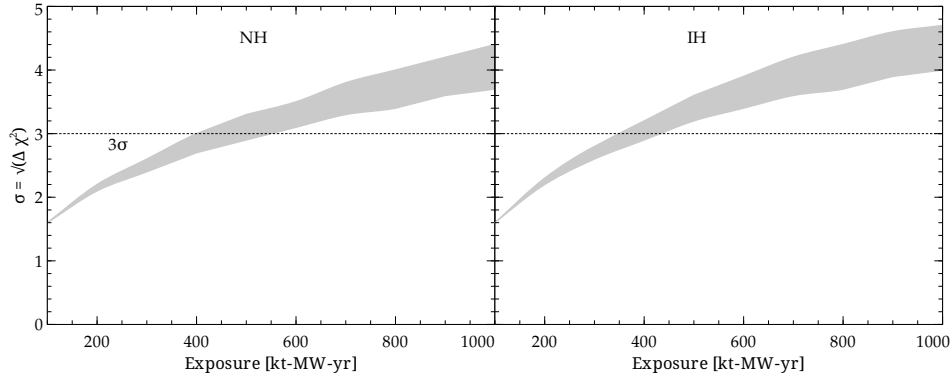


Fig. 15. Similar to Figs. 4 and 11, but for the maximum sensitivity to CP violation for 70% of the δ_{CP} parameter space.

than about 35 kt-MW-yr. The sensitivity gradually increases with exposure and the CP fraction for which 3σ sensitivity is achieved approaches 0.4 (without an ND) and 0.5 (with an ND) for a 125 kt-MW-yr exposure. The CP fraction plateaus to a value below 0.8 for an exposure of 350 kt-MW-yr with all data combined.

- A near detector certainly improves the sensitivity to CP violation.

5.3. Variation of systematics

Figure 15 shows the maximum sensitivity to CP violation that can be achieved for 70% of the δ_{CP} parameter space. As in Figs. 4 and 11, we show the sensitivity as a band on varying the systematics. The notable features of Fig. 15 are,

- To resolve CP violation at the level of 3σ for 70% region of the δ_{CP} space, a fairly long exposure is needed. For NH, it is roughly 400 – 500 kt-MW-yr. while for IH it is 350 – 450 kt-MW-yr. depending on the systematics.)
- For such long exposures, the sensitivity band becomes appreciably wide indicating a strong dependence on the systematics. In comparison, the sensitivities to the mass hierarchy and octant were less dependent on systematics since the corresponding exposures were smaller. This reinforces the need for an ND.

5.4. Effect of magnetization

As can be seen from Fig. 13, the sensitivity of atmospheric neutrinos to CPV is negligible, hence magnetizing the detector does not help.

It is obvious that CP-violation is the study that stands to benefit most from the combination of results from the T2K, NO ν A and the DUNE. Even potentially low sensitivity to maximal CP-violation due to the absence of ND can be overcome by the combination of χ^2 data from the three experiments. However, a large volume FD (35 kt) for the DUNE is almost certainly an absolute necessity, if any sensitivity to CP-violation has to be detected within a reasonable time frame, irrespective of the benefits of combining results from other experiments such as the T2K and NO ν A.

The atmospheric neutrino flux has no role to play in the resolution of this physical problem.

6. Summary

We considered the Deep Underground Neutrino Experiment as either a 10 kt or 35 kt LAr detector situated underground at the Homestake mine and taking data in a high intensity neutrino beam for 5 years and in an antineutrino beam for another 5 years. For the 35 kt detector, we find that reduced systematic uncertainties afforded by a near detector greatly benefit the sensitivity to CP violation. However, a near detector provides only modest help with the octant degeneracy and is not necessary for the determination of the mass hierarchy since the sensitivity without a near detector is well above 5σ . Since magnetization is not currently feasible for a 35 kt detector, we only considered this possibility for a 10 kt detector. While the sensitivity to the mass hierarchy from atmospheric neutrinos gets enhanced to almost 3σ , the combined beam and atmospheric data is not much affected by magnetization. Also, magnetizing the detector does not help improve the sensitivity to the octant or to CP violation.

One thing is clear. A 35 kt DUNE will break all remaining vestiges of the eight-fold degeneracy that plagues long-baseline beam experiments²⁰ and will answer all the questions it is designed to address.

Acknowledgments

AB, AC, RG and MM thank Pomita Ghoshal and Sanjib Mishra for discussions. This work was supported by US DOE grants DE-FG02-95ER40896 and de-sc0010504. RG acknowledges the support of the XI Plan Neutrino Project under DAE.

Appendix

7. Atmospheric neutrino analysis

The simulation of atmospheric neutrino events and the subsequent χ^2 analysis is carried out by means of a C++ program. Our method is described below.

7.1. Event simulation

The total number of CC events is obtained by folding the relevant incident neutrino fluxes with the appropriate disappearance and appearance probabilities, relevant

CC cross sections, and the detector efficiency, resolution, mass, and exposure time. For our analysis, we consider neutrinos with energy in the range 1–10 GeV in 10 uniform bins, and the cosine of the zenith angle θ in the range -1.0 to -0.1 in 18 bins. The μ^- event rate in an energy bin of width dE and in a solid angle bin of width $d\Omega$ is,

$$\frac{d^2N_\mu}{d\Omega dE} = \frac{1}{2\pi} \left[\left(\frac{d^2\Phi_\mu}{d \cos \theta dE} \right) P_{\mu\mu} + \left(\frac{d^2\Phi_e}{d \cos \theta dE} \right) P_{e\mu} \right] \sigma_{CC} D_{\text{eff}}. \quad (7)$$

Here Φ_μ and Φ_e are the ν_μ and ν_e atmospheric fluxes, $P_{\mu\mu}$ and $P_{e\mu}$ are disappearance and appearance probabilities in obvious notation, σ_{CC} is the total CC cross section and D_{eff} is the detector efficiency. The μ^+ event rate is similar to the above expression with the fluxes, probabilities and cross sections replaced by those for antimuons. Similarly, the e^- event rate in a specific energy and zenith angle bin is

$$\frac{d^2N_e}{d\Omega dE} = \frac{1}{2\pi} \left[\left(\frac{d^2\Phi_\mu}{d \cos \theta dE} \right) P_{\mu e} + \left(\frac{d^2\Phi_e}{d \cos \theta dE} \right) P_{ee} \right] \sigma_{CC} D_{\text{eff}}, \quad (8)$$

with the e^+ event rate being expressed in terms of antineutrino fluxes, probabilities and cross sections.

We take into account the smearing in both energy and zenith angle, assuming a Gaussian form for the resolution function, R . For energy, we use,

$$R_E(E_t, E_m) = \frac{1}{\sqrt{2\pi}\sigma} \exp \left[-\frac{(E_m - E_t)^2}{2\sigma^2} \right]. \quad (9)$$

Here, E_m and E_t denote the measured and true values of energy respectively. The smearing width σ is a function of E_t .

The smearing function for the zenith angle is a bit more complicated because the direction of the incident neutrino is specified by two variables: the polar angle θ_t and the azimuthal angle ϕ_t . We denote both these angles together by Ω_t . The measured direction of the neutrino, with polar angle θ_m and azimuthal angle ϕ_m , which together we denote by Ω_m , is expected to be within a cone of half angle $\Delta\theta$ of the true direction. The angular smearing is done in a small cone whose axis is given by the direction θ_t, ϕ_t . The set of directions within the cone have different polar angles and azimuthal angles. Therefore, we need to construct a smearing function which takes into account the change in the azimuthal coordinates as well. Such an angular smearing function is given by,

$$R_\theta(\Omega_t, \Omega_m) = N \exp \left[-\frac{(\theta_t - \theta_m)^2 + \sin^2 \theta_t (\phi_t - \phi_m)^2}{2(\Delta\theta)^2} \right], \quad (10)$$

where N is a normalisation constant.

Now, the ν_μ event rate with the smearing factors taken into account is given by,

$$\frac{d^2N_\mu}{d\Omega_m dE_m} = \frac{1}{2\pi} \int \int dE_t d\Omega_t R_{EN}(E_t, E_m) R_\theta(\Omega_t, \Omega_m) [\Phi_\mu^d P_{\mu\mu} + \Phi_e^d P_{e\mu}] \sigma_{CC} D_{\text{eff}}, \quad (11)$$

and similarly for the ν_e event rate. We have introduced the notation,

$$(d^2\Phi/d\cos\theta dE)_{\mu,e} \equiv \Phi_{\mu,e}^d.$$

Since $R_{EN}(E_t, E_m)$ and $R_\theta(\Omega_t, \Omega_m)$ are Gaussian, they can easily be integrated over the true angle Ω_t and the true energy E_t . Then, integration over the measured energy E_m and measured angle Ω_m is carried out using the VEGAS Monte Carlo Algorithm.

7.2. χ^2 analysis

The computation of χ^2 for a fixed set of parameters is performed using the method of pulls. This method allows us to take into account the various statistical and systematic uncertainties in a straightforward way. The flux, cross sections and other systematic uncertainties are included by allowing these inputs to deviate from their standard values in the computation of the expected rate in the i - j th bin, N_{ij}^{th} . Let the k th input deviate from its standard value by $\sigma_k \xi_k$, where σ_k is its uncertainty. Then the value of N_{ij}^{th} with the modified inputs is

$$N_{ij}^{\text{th}} = N_{ij}^{\text{th}}(\text{std}) + \sum_{k=1}^{\text{npull}} c_{ij}^k \xi_k, \quad (12)$$

where $N_{ij}^{\text{th}}(\text{std})$ is the expected rate in the i - j th bin calculated with the standard values of the inputs and npull is the number of sources of uncertainty, which is 5 in our case. The ξ_k 's are called the *pull* variables and they determine the number of σ 's by which the k th input deviates from its standard value. In Eq. (12), c_{ij}^k is the change in N_{ij}^{th} when the k th input is changed by σ_k (*i.e.* by 1 standard deviation). Since the uncertainties in the inputs are not very large, we only consider changes in N_{ij}^{th} that are linear in ξ_k . Thus we have the modified χ^2 ,

$$\chi^2(\xi_k) = \sum_{i,j} \frac{\left[N_{ij}^{\text{th}}(\text{std}) + \sum_{k=1}^{\text{npull}} c_{ij}^k \xi_k - N_{ij}^{\text{ex}} \right]^2}{N_{ij}^{\text{ex}}} + \sum_{k=1}^{\text{npull}} \xi_k^2, \quad (13)$$

where the additional ξ_k^2 -dependent term is the penalty imposed for moving the value of the k th input away from its standard value by $\sigma_k \xi_k$. The χ^2 with pulls, which includes the effects of all theoretical and systematic uncertainties, is obtained by minimizing $\chi^2(\xi_k)$ with respect to all the pulls ξ_k :

$$\chi_{\text{pull}}^2 = \text{Min}_{\xi_k} [\chi^2(\xi_k)]. \quad (14)$$

In the calculation of χ_{pull}^2 , we consider uncertainties in the flux, cross sections etc. (as in Table 6), keeping the values of the oscillation parameters fixed while calculating N_{ij}^{ex} and N_{ij}^{th} . However, in general, the values of the mass-squared difference Δm_{31}^2 and the mixing angles θ_{23} and θ_{13} can vary over a range corresponding to the actual measurements of these parameters. Holding them fixed at particular

Table 6. Uncertainties for various quantities.¹⁸

Quantity	Value
Flux normalization uncertainty	20%
Zenith angle dependence uncertainty	5%
Cross section uncertainty	10%
Overall systematic uncertainty	5%
Tilt uncertainty	$\Phi_\delta \approx \Phi_0(E) \left[1 + \delta \log \left(\frac{E}{E_0} \right) \right]$ with $E_0 = 2$ GeV, $\sigma_\delta = 5\%$ (see, e.g., ²¹)

values is equivalent to knowing the parameters to infinite precision, which is obviously unrealistic. To take into account the uncertainties in the actual measurement of the oscillation parameters, we define the marginalized χ^2 as¹⁸

$$\chi_{\min}^2 = \text{Min} \left[\chi^2(\xi_k) + \left(\frac{|\Delta m_{31}^2|^{\text{true}} - |\Delta m_{31}^2|}{\sigma(|\Delta m_{31}^2|)} \right)^2 + \left(\frac{\sin^2 2\theta_{23}^{\text{true}} - \sin^2 2\theta_{23}}{\sigma(\sin^2 2\theta_{23})} \right)^2 + \left(\frac{\sin^2 2\theta_{13}^{\text{true}} - \sin^2 2\theta_{13}}{\sigma(\sin^2 2\theta_{13})} \right)^2 \right]. \quad (15)$$

The three terms added to $\chi^2(\xi_k)$ are known as *priors*. Now, for our χ^2 analysis, we proceed as follows, e.g. for the case of the mass hierarchy.

- Our aim is to see at what statistical significance the *wrong hierarchy* can be ruled out. Our procedure gives the median sensitivity of the experiment in the frequentist approach.²²
- We simulate the number of events in 10 bins in the measured energy E_m and 18 bins in the measured zenith angle $\cos \theta_m$ for a set of *true values* for the six neutrino parameters: θ_{12} , θ_{23} , θ_{13} , Δm_{21}^2 , Δm_{31}^2 , δ_{CP} , and for a *true hierarchy*. The *true values* are the current best fit values of the oscillation parameters and the true value of δ_{CP} is assumed to be zero. This is our *experimental data* – N_{ij}^{ex} . Now we calculate the *theoretical expectation* in each bin – N_{ij}^{th} assuming the *wrong hierarchy*, and calculate the χ^2 between these two datasets.
- For the marginalization procedure, we allow θ_{23} , θ_{13} , $|\Delta m_{31}^2|$ and δ_{CP} to vary within the following ranges:

$$\theta_{23} \in [36^\circ, 54^\circ],$$

$$\theta_{13} \in [5.5^\circ, 11^\circ],$$

$$|\Delta m_{31}^2| \in [2.19, 2.62] \times 10^{-3} \text{ eV}^2,$$

$$\delta_{\text{CP}} \in [-\pi, \pi].$$
- In computing χ_{\min}^2 , we add the priors for the neutrino parameters which assigns a penalty for moving away from the true value. During marginalization, as the value of an oscillation parameters shifts further from its true value, Eq. (15) suggests that the corresponding prior will be larger resulting

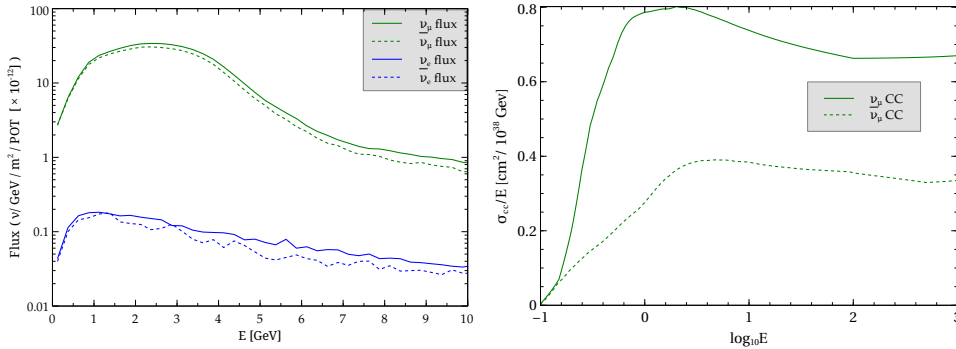


Fig. 16. The neutrino and antineutrino fluxes are shown in the left panel. The right panel shows the ν and $\bar{\nu}$ charged current cross sections.

in a higher χ^2 value.

- Finally, after adding the priors, we determine χ^2_{pull} (see Eq. 14). This is a multi-dimensional parameter space minimization of the function $\chi^2(\alpha, \beta, \dots)$, where α, β, \dots are the parameters over which marginalization is required. For the purpose of this multi-minimization, we have used the NLOpt library.²³ We do the minimization first over the entire multi-dimensional parameter space to locate the global minimum approximately, and then use the parameters corresponding to this as a guess to carry out a local minimum search to locate the minimized χ^2 within the parameter space accurately. We carry out this minimization routine using a simplex algorithm described in Ref.²⁴, and implemented within the NLOpt library.

8. DUNE fluxes and atmospheric neutrino events

The fluxes and charged current cross sections used in our analysis are shown in Fig. 16. These are similar to those used by the DUNE collaboration.

In Fig. 17, we show the number of ν_μ and ν_e atmospheric events with and without oscillations for an exposure of 350 kt-yr.

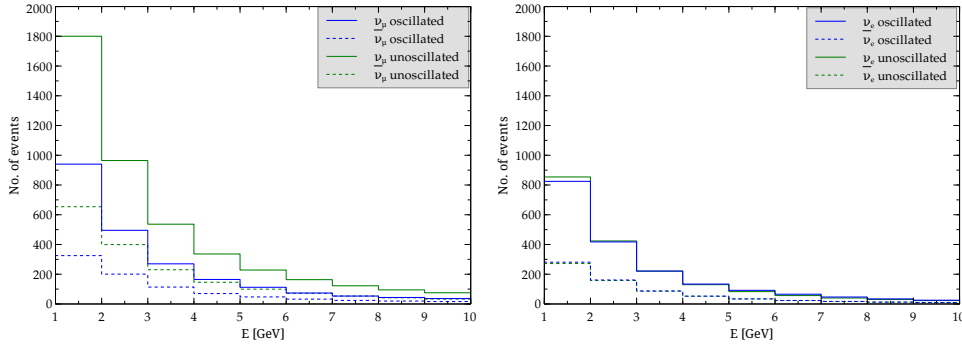


Fig. 17. ν_μ (left panel) and ν_e (right panel) atmospheric events for a 350 kt-yr LAr FD.

References

1. F. An *et al.* [Daya-Bay Collaboration], *Chin. Phys. C* **37**, 011001 (2013); *Phys. Rev. Lett.* **108**, 171803 (2012) [arXiv:1203.1669 [hep-ex]]; J. Ahn *et al.* [RENO Collaboration], *Phys. Rev. Lett.* **108**, 191802 (2012); Y. Abe *et al.* [Double Chooz Collaboration], *Phys. Rev. D* **86**, 052008 (2012) [arXiv:1207.6632 [hep-ex]].
2. G. Fogli, E. Lisi, A. Marrone, D. Montanino, A. Palazzo and A. Rotunno, *Phys. Rev. D* **86**, 013012 (2012) [arXiv:1205.5254 [hep-ph]].
3. K. Abe *et al.* [T2K Collaboration], *Phys. Rev. D* **88**, 032002 (2013) [arXiv:1304.0841 [hep-ex]].
4. C. Adams *et al.* [LBNE Collaboration], arXiv:1307.7335 [hep-ex].
5. T. Akiri *et al.* [LBNE Collaboration], arXiv:1110.6249 [hep-ex].
6. Physics Working Group Report to the LBNE Reconfiguration Steering Committee, http://www.fnal.gov/directorate/lbne_reconfiguration/files/LBNE-Reconfiguration-PhysicsWG-Report-August2012.pdf
7. V. Barger, A. Bhattacharya, A. Chatterjee, R. Gandhi, D. Marfatia and M. Masud, *Phys. Rev. D* **89**, 011302 (2014) [arXiv:1307.2519 [hep-ph]].
8. M. Bass, D. Cherdack and R. J. Wilson, arXiv:1310.6812 [hep-ex]; K. Bora and D. Dutta, arXiv:1209.1870 [hep-ph]; S. Agarwalla, *Adv. High Energy Phys.* **2014**, 457803 (2014) [arXiv:1401.4705 [hep-ph]]; S. Agarwalla, S. Prakash and S. U. Sankar, *JHEP* **1403**, 087 (2014) [arXiv:1304.3251 [hep-ph]]; C. Bromberg, *PoS DSU* **2012**, 036 (2012).
9. D. Ayres *et al.* [NOvA Collaboration], hep-ex/0503053.
10. Y. Itow *et al.* [T2K Collaboration], hep-ex/0106019.
11. V. Barger, P. Huber, D. Marfatia and W. Winter, *Phys. Rev. D* **76**, 031301 (2007) [hep-ph/0610301].
12. S. K. Agarwalla, S. Prakash, S. K. Raut and S. U. Sankar, *JHEP* **1212**, 075 (2012) [arXiv:1208.3644 [hep-ph]].
13. P. Huber, J. Kopp, M. Lindner, M. Rolinec and W. Winter, *Comput. Phys. Commun.* **177**, 432 (2007).
14. V. Barger, P. Huber, D. Marfatia and W. Winter, *Phys. Rev. D* **76**, 053005 (2007) [hep-ph/0703029].
15. S. Mishra, private communication.
16. V. Barger, R. Gandhi, P. Ghoshal, S. Goswami, D. Marfatia, S. Prakash, S. Raut and

- S. U. Sankar, Phys. Rev. Lett. **109**, 091801 (2012).
17. M. Honda, T. Kajita, K. Kasahara and S. Midorikawa, Phys. Rev. D **70** (2004) 043008.
 18. R. Gandhi, P. Ghoshal, S. Goswami, P. Mehta, S. U. Sankar and S. Shalgar, Phys. Rev. D **76**, 073012 (2007) [arXiv:0707.1723 [hep-ph]].
 19. A. Dziewonski and D. Anderson, Phys. Earth Planet. Interiors **25** (1981) 297.
 20. V. Barger, D. Marfatia and K. Whisnant, Phys. Rev. D **65**, 073023 (2002) [hep-ph/0112119].
 21. M. C. Gonzalez-Garcia and M. Maltoni, Phys. Rev. D **70**, 033010 (2004) [hep-ph/0404085].
 22. M. Blennow, P. Coloma, P. Huber and T. Schwetz, JHEP **1403**, 028 (2014) [arXiv:1311.1822 [hep-ph]].
 23. S. Johnson, *The NLOpt nonlinear-optimization package*, <http://ab-initio.mit.edu/nlopt>
 24. J. Nelder and R. Mead, Computer Journal **308** (1965) 7.